Energy & Environmental Science

Volume 1 | Number 1 | Jan 2013 | Pages 1–100

www.rsc.org/ees

ROYAL SOCIETY OF CHEMISTRY

This is an *Accepted Manuscript*, which has been through the Royal Society of Chemistry peer review process and has been accepted for publication.

Accepted Manuscripts are published online shortly after acceptance, before technical editing, formatting and proof reading. Using this free service, authors can make their results available to the community, in citable form, before we publish the edited article. We will replace this *Accepted Manuscript* with the edited and formatted *Advance Article* as soon as it is available.

You can find more information about *Accepted Manuscripts* in the **Information for Authors**.

Please note that technical editing may introduce minor changes to the text and/or graphics, which may alter content. The journal's standard **Terms & Conditions** and the **Ethical guidelines** still apply. In no event shall the Royal Society of Chemistry be held responsible for any errors or omissions in this *Accepted Manuscript* or any consequences arising from the use of any information it contains.

Energy & Environmental Science

RSCPublishing

PAPER

A multiple ion-exchange membrane design for redox flow batteries †

Shuang Gu,* Ke Gong, Emily Z. Yan, and Yushan Yan*

Here we present a multiple ion-exchange membrane (IEM) cell design for redox flow batteries (RFBs) that can generally accommodate redox pair combinations with any mixed ion charges. This design also allows flexible choice of electrolytes such as acid electrolyte at one electrode while base in the other. More specifically, the double-IEM cell with one anion-exchange membrane (AEM), one cation-exchange membrane (CEM), and a middle electrolyte in between, can work with all redox pairs except the case of two hybrid redox pairs (i.e., an anion-cation pair vs. an anion-cation pair). For the combination of two hybrid pairs, a triple-IEM cell with three membranes (CEM/AEM/CEM or AEM/CEM/AEM) and two middle electrolytes is needed. The double- and triple-IEM cells bring unprecedented freedom in choosing redox pairs and supporting electrolytes. Of particular importance, two featured aqueous RFBs are demonstrated here: (1) ultra-high voltage zinc-cerium RFB with 3.08 V standard cell voltage, the highest among all known aqueous RFBs; and (2) ultra-low cost sulfur-iron RFB with 1.22 V standard cell voltage, with two highly available elements (iron and sulfur are the 1st and 5th most produced elements worldwide, respectively).

Introduction

The first redox flow battery (i.e., chromium-iron RFB) was invented in 1974 [1]. Its key feature was that an ion-exchange membrane (IEM), positioned in the middle of a battery cell, isolated negative electrode redox pair (negative pair) from positive electrode redox pair (positive pair) even when all of the four redox ions were freely dissolved in electrolytes [2, 3]. Equally importantly, the IEM also allowed the passage of non-electroactive counter ions to balance the charge between negative and positive electrolytes. The liberation of redox pairs from the solid electrodes enabled the transfer of energy storage function from electrodes to liquid electrolytes in external tanks, and this decoupling of energy storage from power delivery provided RFBs with unprecedented design flexibility and scalability. Significant efforts and progresses have been made in developing efficient and economical RFB systems in the last two decades mostly

Department of Chemical & Biomolecular Engineering, Center for Catalytic Science and Technology, University of Delaware, Newark, DE 19716, USA.

Correspondence and requests for materials should be addressed to Shuang Gu (email: shgu@udel.edu) or Yushan Yan (email: yanys@udel.edu).

† Electronic Supplementary Information (ESI) available: Text S1, Tables S1-S2, and Figures S1-S5. See DOI: 10.1039/b000000x/

driven by increased use of intermittent renewable energy sources like wind and solar [4-22].

In the original chromium-iron RFB design, one anion-exchange membrane (AEM) was used to isolate the cation/cation negative pair (i.e., Cr^{3+}/Cr^{2+}) from the cation/cation positive pair (i.e., Fe^{3+}/Fe^{2+}) to prevent self-discharge while allowing the conduction of the non-electroactive anions (i.e., Cl^- in HCl solution) to balance the charges between two electrolytes. Similarly, one cation-exchange membrane (CEM) can work for the cell with an anion/anion negative pair and an anion/anion positive pair. However, neither one single AEM nor one single CEM can effectively prevent the mixing of electroactive redox pairs with mixed ion charges [23-26], in spite of the fact that some of these mixed ion pairs can lead to RFBs with potentially higher performance and lower cost. Examples of charge-mixed ion pairs separated by a single membrane (AEM, CEM, or non-ion-selective porous membrane) include a RFB with cation/cation negative pair (e.g., V^{3+}/V^{2+}) and anion/anion positive pair (e.g., $ClBr_2^-/Br^-$) [25, 26]. A membrane-free cell configuration was also explored for a RFB with $Cr(edta)^-/Cr(edta)^{2-}$ as negative pair and $Cr(edta)^+/Cr(edta)^-$ as positive pair [24]. Overall, the energy efficiency of these RFBs is limited (membrane-free: 7%; non-ion-selective porous membrane: 38−56%; single AEM: 36%; single CEM: 27%−66%, albeit the redox pairs and test conditions were somewhat different).

Early in 2013, a bipolar-IEM (one side being AEM and the other being CEM with no gap in between) was introduced by K.Y. Chan and co-workers in a semi-RFB (a non-flow metal hydride negative electrode combined with a flow vanadium positive electrode) [27, 28]. In principle, the bipolar IEM cell configuration can

isolate the anion/anion redox pair from cation/cation redox pair, but the charge communication between the two electrolytes is expected to be fundamentally limited by water dissociation inside bipolar membrane (i.e., high current density operation is subject to a substantial voltage penalty [29-32]). In addition, the electrolyte selection is also limited, since proton (H^+) and hydroxide (OH^-) are required to be charge carriers in the bipolar-IEM (H^+ for CEM side and OH^- for AEM side)[33, 34]. A modified bipolar membrane configuration has also been introduced in fuel cells for improved water management[35, 36]. On the other hand, it is known in electrodialysis industry that coupling one AEM and one CEM together with a middle electrolyte in between can effectively separate ions with mixed charges and also provide efficient charge communication between two electrolytes[37]. The charge carriers in double-IEM are not limited to proton and hydroxide, thus eliminating the limitation of electrolyte selection faced by bipolar-IEM cell configuration. In addition, the double-IEM cell configuration has also been introduced and traditional rechargeable batteries [32, 38]; and these successes suggest the feasibility of introducing multiple IEMs with middle electrolyte(s) in RFBs with redox pairs of mixed charges for both redox ion isolation and electrolyte charge communication.

Here we present a general multiple-IEM RFB cell design that can accommodate any redox pair combinations of mixed ion charges for both the negative and the positive pairs. Composed of one AEM, one CEM, and a middle electrolyte in between, the double-IEM cell configuration provides a solution for redox pairs of all combinations of ion charges except the combination of two hybrid pairs (i.e., an anion-cation pair vs. another anion-cation pair). For the case of two hybrid pairs, a triple-IEM cell configuration with three membranes (CEM/AEM/CEM or AEM/CEM/AEM) and two middle electrolytes is needed. The multiple-IEM (double-IEM and triple-IEM) designs bring unprecedented freedom in choosing redox pairs and electrolytes, and of particular importance, two featured aqueous RFBs are demonstrated here: (i) **ultra-high voltage zinc-cerium RFB** with 3.08 V of standard cell voltage ($Zn(OH)_4^{2-}/Zn$ anion redox pair combined with Ce_2O^{6+}/Ce^{3+} cation redox pair); and (ii) **ultra-low cost sulfur-iron RFB** with 1.22 V of standard cell voltage (S_4^{2-}/S_2^{2-} anion redox pair combined with Fe^{3+}/Fe^{2+} cation redox pair), with two highly-available elements (iron and sulfur are the, 1st and 5th most produced element worldwide).

Experimental

Experimental double-IEM RFB cell

The three-compartment cell was constructed by three rectangular acrylic frames (3 cm * 4 cm of open area, 5 cm * 6 cm of overall area, and 1 cm of thickness). A negative electrode, a CEM, an AEM, and a positive electrode were assembled in sequence to form the three compartments (negative, middle, and positive compartment). Silicone gaskets were attached to both sides of acrylic frames to seal each compartment, and the whole cell was tightly compressed by four screws. The whole test cell is shown in **Fig. S5**. Every cell compartment was connected by two PTFE-lined rubber tubes (inlet and outlet holes in acrylic frame) to its corresponding external electrolyte tank (25 ml each). The flow rate of electrolytes passing through the cell compartment was controlled by a peristaltic pump (Masterflex® L/S® 100RPM). The negative and positive electrodes were connected to a potentiostat/galvanostat (Solartron 1287A) for cell performance tests. Nafion® 1135 membrane, (DuPont, 88 µm thickness) and Fumasep® FAA membrane (Fuma-Tech, 70 µm thickness) were used as the CEM and AEM, respectively, in the double-IEM cell.

Fabrication of the zinc-cerium double-IEM RFB

0.5 M $Na_2[Zn(OH)_4]$ containing 3 M NaOH was used as the initial negative electrolyte (prepared by dissolving ZnO into NaOH solution [39]). 0.5 M $Ce(ClO_4)_3$ containing 2.5 M $HClO_4$ was used as the initial positive electrolyte (prepared by dissolving $Ce_2(CO_3)_3$ into perchloric acid solution, similar to the method in the reference [40]). 4 M $NaClO_4$ was used as the middle electrolyte. The volume for each electrolyte used in test was 25 ml. A rectangular cadmium-plated copper plate (5 cm * 6 cm, 0.5 mm thickness) was used as the negative electrode and current collector as well. The cadmium plating (3 µm on average) on the copper plate (ESPI Metals, 3N grade) was carried out according to a published method[39]. A carbon felt (3 cm * 4 cm, 1 mm total thickness, Sigracell® GFA5 EA type) was used as the positive electrode where a graphite plate (5 cm * 6 cm, 1 mm thickness, SGL Group, Sigracet® TF6 type) was used its current collector.

Flow battery test of the zinc-cerium double-IEM RFB

Open circuit voltage (OCV) was measured after charging the cell to 90% SOC at 5 mA/cm² current density (20 ml/min of flow rate for all three electrolytes). The charge curve was obtained by charging the cell from the initial zero to 75% state of charge (SOC) with the same current density and flow rate; and the discharge curve was obtained by discharging the above charged cell to the cut-off cell voltage of 1.80 V (almost completely discharged). The deep cycling test was performed by alterative charge and discharge operation, where 0−75% SOC swing was adopted for every cycle by monitoring the cut-off voltages (1.80 and 3.23 V for discharge and charge operation, respectively).

Fabrication of the sulfur-iron double-IEM RFB

1 M Na_2S_4 containing 1 M NaOH was used as the initial negative electrolyte (prepared by dissolving sulfur into Na_2S solution). 1 M $FeCl_2$ containing 1 M HCl was used as the initial positive electrolyte (prepared by dissolving $FeCl_2$ into HCl solution). 3 M NaCl was used as the middle electrolyte. The volume for each electrolyte used in test was 12 ml. Sulfur treated-nickel foam was used as negative electrode (prepared according to the reference [41]) with a rectangular cobalt plate (5 cm * 6 cm, 0.5 mm thickness) as the current collector. A carbon felt (3 cm * 4 cm, 1 mm total thickness, Sigracell® GFA5 EA type) was used as the positive electrode with a graphite plate (5 cm * 6 cm, 1 mm thickness, SGL Group, Sigracet® TF6 type) as the current collector.

Flow battery test of the sulfur-iron double-IEM RFB

Similar to zinc-cerium RFB test, OCV was measured after charging the cell to 90% SOC at 5 mA/cm² current density (20 ml/min of flow rate for all three electrolytes). The charge curve was obtained by charging the cell from the initial zero to 75% SOC (the same current density and flow rate); and the discharge curve was obtained by discharging the above charged cell to the cut-off cell voltage of 0.60 V (almost completely discharged). The deep cycling test was performed by alterative charge and discharge operation, where 0−75% SOC swing was adopted for every cycle by keeping the charge time the same (4 hours).

Results

Working principles and general applicability of double-IEM cell configuration

The double-IEM RFB is shown in **Fig. 1**, consisting of a CEM, an MX solution (middle electrolyte), and an AEM sequentially placed between negative and positive electrode. The working principles of the double-IEM configuration for three RFB combinations are illustrated in **Fig. 2**. For the RFB combination of an anion/anion redox pair vs. a cation/cation redox pair, represented by $A_N^{2-}/A_N^-||C_P^{2+}/C_P^+$ (the double vertical lines representing the double-IEM), its working principle is illustrated in **Fig. 2A**. Note that a single electron transfer was assumed for all redox reactions for simplicity. M^+ and X^- are non-electroactive balancing ions. When the cell is being charged, A_N^- are reduced into A_N^{2-} in negative electrode and C^+ are oxidized into C^{2+} in positive electrode. Meanwhile, M^+ cations cross the CEM from middle electrolyte to negative electrolyte, and X^- anions pass the AEM from middle electrolyte to positive electrolyte. During the charging process, the MX concentration decreases in middle electrolyte. When the cell is being discharged, the opposite processes happen. If a cation/cation pair is used in negative electrolyte and an anion/anion redox pair used in positive electrolyte, the IEM sequence needs to be reversed from CEM-middle electrolyte-AEM to AEM-middle electrolyte-CEM.

The double-IEM configuration can also be applied to RFBs with an anion/anion vs. an anion-cation hybrid pair (i.e., anion/cation or cation/anion) (**Fig. 2B**) or a cation/cation pair vs. an anion-cation hybrid pair (**Fig. 2C**). Taking anion/anion pair vs. cation/anion hybrid pair (e.g., the abovementioned $Cr(edta)^-/Cr(edta)^{2-}$ vs. $Cr(edta)^+/Cr(edta)^-$) as an example (**Fig. 2B**), the AEM can block the electroactive cation of the cation/anion hybrid pair and allow its balancing anion (X_p^-) as well as the electroactive anion (A_p^-) to pass into the middle electrolyte; and the CEM can prevent those anions from passing into the negative electrolyte. As a result of the double-IEM design, the mixing of electroactive ions is avoided.

Zinc-cerium RFB: an ultra-high voltage application of double-IEM cell design

In addition to the freedom in choosing the redox pairs, the double-IEM configuration offers unprecedented freedom in selecting supporting electrolytes such as strong base in the negative electrode and strong acid in the positive electrode. The combination of these two features enables high cell voltages that cannot be achieved with the traditional single-IEM configuration. A high voltage is important for RFBs as it can directly translate into high power density (with the same current density) and high energy density (with the same ion concentration in electrolytes). Specifically, the double-IEM configuration allows a strongly-basic negative electrolyte and a strongly-acidic positive electrolyte to be used in the same RFB cell with a neutral middle electrolyte in between. Consequently, a very negative redox pair and a very positive redox pair can be used to provide ultra-high cell voltage. For example, a basic zinc-acidic cerium RFB $[Zn(OH)_4^{2-}/Zn||Ce_2O^{6+}/Ce^{3+}]$ has been fabricated and demonstrated to have a 3.08 V standard cell voltage by combining the very negative redox potential from $Zn(OH)_4^{2-}/Zn$ in base (−1.21 V) [42] and the very positive redox potential from Ce_2O^{6+}/Ce^{3+} in acid (+1.87 V) [43]. To the best of our knowledge, this cell voltage is the highest among all known aqueous RFBs reported. It is 2.6 times that of chromium-iron RFB (1.18 V) [1], 2.5 times that of all-vanadium RFB (1.25 V) [44], or 2.1 times that of sulfur-bromine RFB (1.50 V) [45]. The cell voltages of reported aqueous RFBs are shown in **Fig. 3**.

As expected, a stable open circuit voltage (OCV) of 3.1 V was observed in the basic zinc-acidic cerium RFB (90% of state of charge, SOC, **Fig. 4A**). The observed high and stable OCV validates the double-IEM concept and its capability of effectively coupling redox pairs with mixed ion charges and pH-different electrolytes. Equally importantly, both discharge and charge operations have been conducted (8-hr charge-discharge cycle and 0−75% SOC swing, **Fig. 5B**). With a constant current density (5 mA/cm²), the cell voltage smoothly increased from 3.1 V to 3.2 V during a 4-hr charge operation; and it smoothly decreased from 2.9 V to 2.7 V after a discharge operation of 3 hrs and 50 mins and then dropped precipitously when the active species mostly converted. A round-trip voltage efficiency of 91% was obtained for the entire charge-discharge cycle, and a round-trip coulombic efficiency as high as 98% was also achieved, confirming the excellent redox pair isolation function of the double-IEM configuration. The overall energy efficiency was close to 90%. In addition, the double-IEM cell is stable, e.g., the overall energy efficiency of the cell remained almost the same during a 50-hr deep cycling test (6 complete cycles with a wide SOC swing of 0-75%, **Fig. 5C**). The cell construction and performance parameters of ultra-high voltage zinc-cerium RFB are shown in **Table 2**.

Note that the high cell voltage of the double-IEM basic zinc-acidic cerium RFB is not compromised by water solvent, as the voltage window of water electrolysis is largely extended. For a single-IEM RFB, its reversible voltage is limited to 1.23 V (e.g., HER, hydrogen evolution reaction, = 0 vs. OER, oxygen evolution reaction, = +1.23 V at pH = 0, or HER = −0.83 vs. OER = +0.40 V at pH = 14), because the same pH has to be maintained in both negative and positive electrolytes. By contrast, a double-IEM cell can have a much larger reversible voltage window of 2.06 V (i.e., HER = −0.83 at pH=14 vs. OER = +1.23 V at pH = 0), owing to the ability to combine strong-base negative electrolyte and strong-acid positive electrolyte. The double-IEM design also took advantage of the fact that the overpotential tolerance to hydrogen evolution side-reaction in base is higher than in acid while the overpotential tolerance to oxygen evolution side-reaction is higher in acid than in base.

Sulfur-iron RFB: an ultra-low cost RFB application of double-IEM cell design

The double-IEM configuration is not limited to the basic zinc-acidic cerium RFB, and many other redox pair combinations are possible. For example, ultra-low cost sulfur-iron RFB was, for the first time, constructed with the double-IEM cell design by using the two highly-available elements of iron and sulfur (1st and 5th most produced element worldwide, respectively). Combining S_4^{2-}/S_2^{2-} anion redox pair (−0.45 V) and Fe^{3+}/Fe^{2+} cation redox pair (+0.77 V), the sulfur-iron RFB has the standard cell voltage of 1.22 V (almost the same as all-vanadium RFB, 1.25 V), but without the concerns of relatively high cost and limited availability of earth-rare vanadium element. Under exactly the same test conditions as zinc-cerium RFB, the sulfur-iron RFB was characterized (**Fig. 5**): A stable OCV of 1.4 V was also obtained (**Fig. 5A**). Both charge and discharge operations were functional (**Fig. 5B**), showing 100%, 70%, and 70% round-trip columbic efficiency, voltage efficiency, and overall energy efficiency, respectively. No obvious energy efficiency loss was found during the 50-hr deep cycling test (**Fig. 6C**). These test results again validate the double-IEM RFB design and its ability to effectively couple redox pairs with mixed ion charges and different electrolytes as well. The cell construction and performance parameters of the ultra-low cost sulfur-iron RFB are also shown in **Table 2**.

This journal is © The Royal Society of Chemistry 2012

Energy & Environ. Sci., 2013, **00**, 1-13 | **3**

Triple-IEM RFB cell configuration

By adding a third IEM to the double-IEM, the triple-IEM configuration with either AEM/CEM/AEM or CEM/AEM/CEM sequence can address the most challenging redox pair isolation problem presented by two anion-cation hybrid pairs. With the third IEM, the middle electrolyte is divided into two electrolytes: left and right middle electrolyte. Taking the triple-IEM combination of AEM/CEM/AEM as an example (**Fig. 6A**), the two AEMs can block the electroactive cations but not the electroactive anion of the negative and positive hybrid pairs. However, the crossed electroactive anions will be stopped by the CEM between the two AEMs. Similarly the triple-IEM combination of CEM/AEM/CEM can also isolate two hybrid pairs (**Fig. 6B**). The preferred cell configurations of typical aqueous RFBs involving anion-cation hybrid redox pair(s) are shown in in **Fig. 4**.
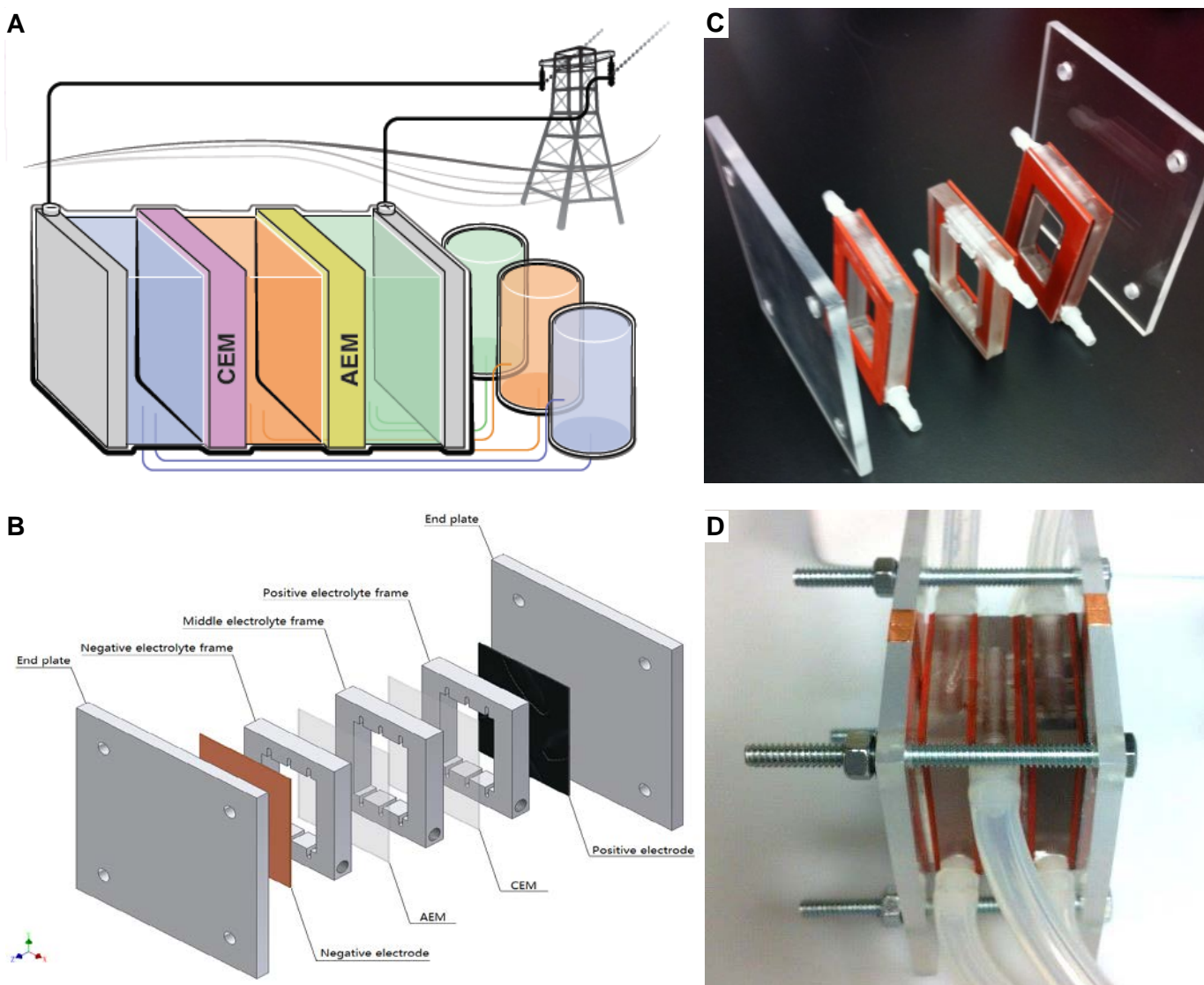

Fig. 1. Double-IEM RFB. It consists of two types of IEMs (one CEM and one AEM) and three separate electrolytes (negative, middle, and positive). (**A**) Concept schematic. (**B**) Cell design. (**C**) Cell components. (**D**) Assembled cell.
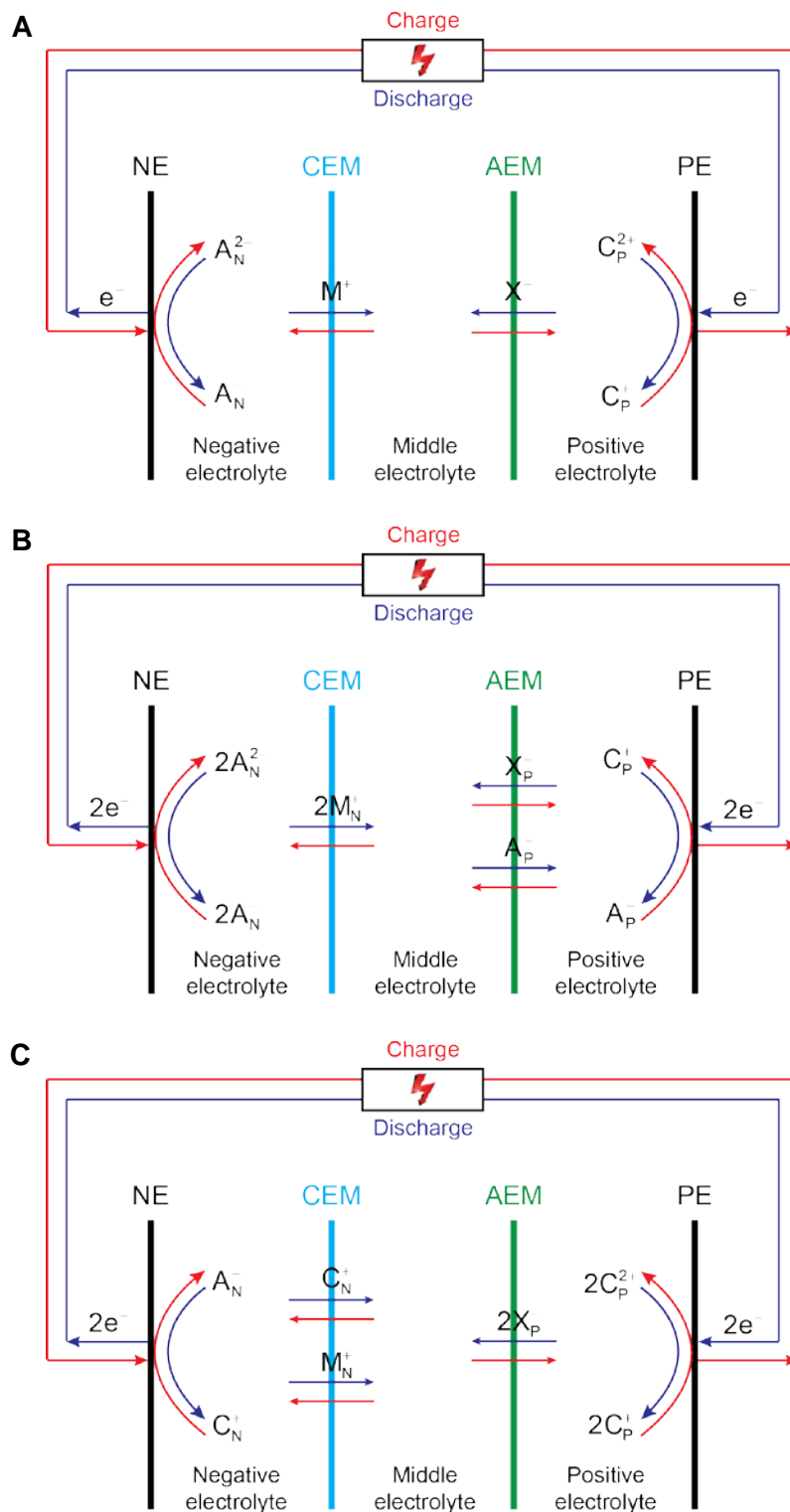
Fig. 2. Working principles of double-IEM RFB cell configuration. NE and PE represent the negative electrode and positive electrode, respectively. (**A**) Combination of an anion-anion (negative) redox pair (A_N^-/A_N^{2-}) and a cation-cation (positive) redox pair (C_P^{2+}/C_P^+). (**B**) Combination of an anion-anion (negative) redox pair (A_N^-/A_N^{2-}) and an anion-cation hybrid (positive) redox pair (C_P^+/A_P^-). (**C**) Combination of an anion-cation hybrid (negative) redox pair (C_N^+/A_N^-) and a cation-cation (positive) redox pair (C_P^{2+}/C_P^+). M^+, X^-, M_N^+, and X_P^- are balancing ions. Note that the general working principles are, for the sake of simplicity, based on the assumptions that cations with more positive charge have higher oxidation number than those with less positive

charge, and anions with more negative charge have lower oxidation number than those with less negative charge. When ions that do not follow those assumptions are used, the working principles are still applicable with minor alterations.
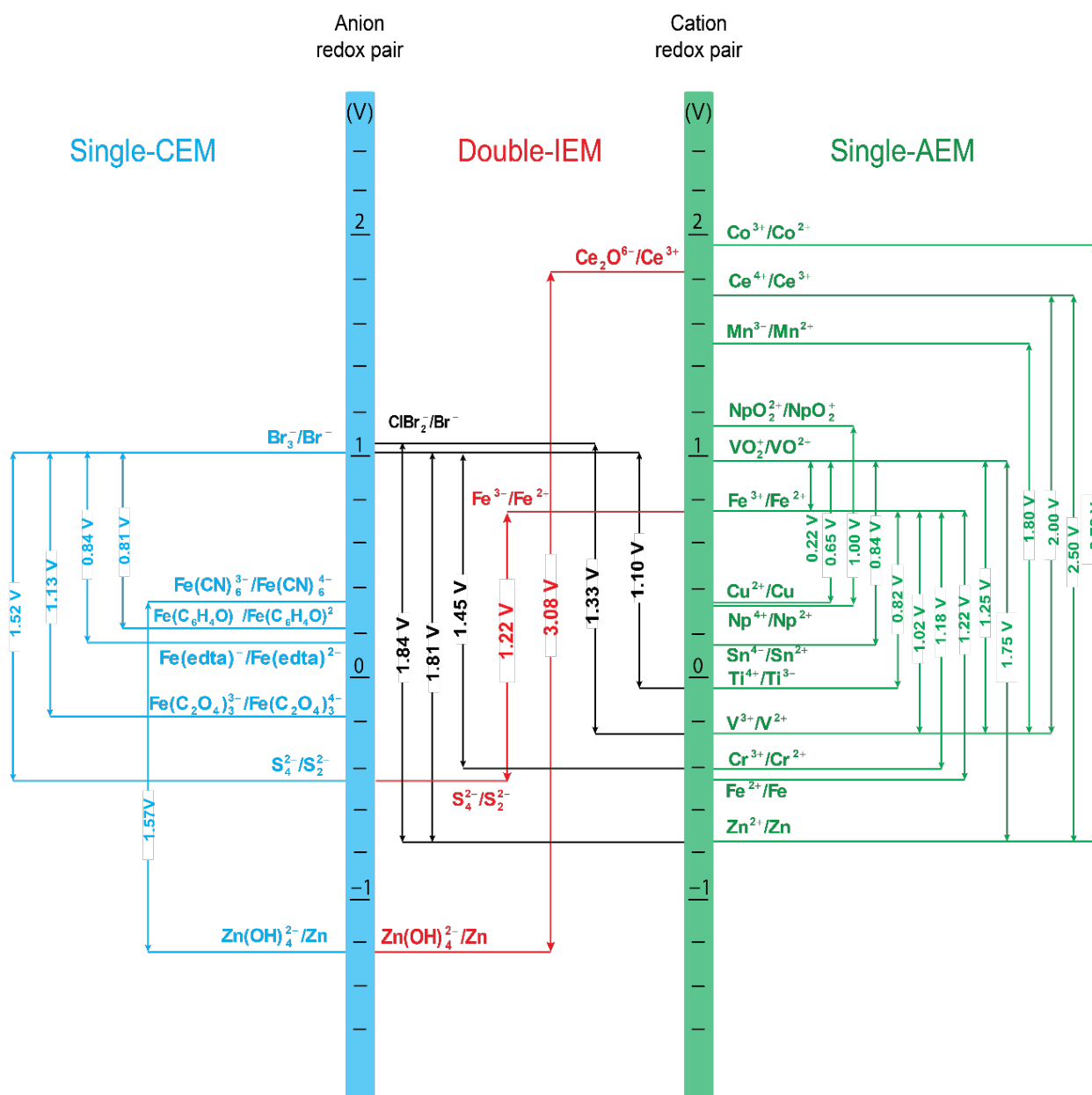

Fig. 3. Preferred cell configurations for aqueous RFBs without anion-cation hybrid redox pairs. The standard redox potentials of redox pairs are from the references in **Table 1**. Single-CEM cell is preferred for one anion-anion redox pair vs. another anion-anion redox pair (left region); single-AEM cell is preferred for one cation-cation redox pair vs. another cation-cation redox pair (right region); and double-IEM cell is preferred for an anion-anion redox pair vs. a cation-cation redox pair (middle region).

6 | *Energy & Environ. Sci.*, 2013, **00**, 1-13

This journal is © The Royal Society of Chemistry 2012

Table 1 Anion-based, cation-based, and anion-cation hybrid redox pairs used in RFBs

Flow battery redox pair		Standard redox potential (V)	Typical electrolyte
Anion-based redox pair	$ClBr_2^-/Br^-$ [25, 46]	+1.07*	HCl, $ZnBr_2$
	Br_3^-/Br^- [45, 47-49]	+1.05*	$NaBr$, H_2SO_4
	$Fe(CN)_6^{3-}/Fe(CN)_6^{4-}$ [50]	+0.36†	$NaOH$
	$Fe(C_6H_4O)^-/Fe(C_6H_4O)^{2-}$ [49]	+0.21†,‡	$NaBr$
	$Fe(edta)^-/Fe(edta)^{2-}$ [23]	+0.18†	$NaAc$
	$Fe(C_2O_4)_3^{3-}/Fe(C_2O_4)_3^{4-}$ [49]	−0.12†	$NaAc$
	S_4^{2-}/S_2^{2-} [45]	−0.45	$NaBr$, $NaOH$
	$Cr(edta)^-/Cr(edta)^{2-}$ [23]	−0.96	$NaAc$
	$Zn(OH)_4^{2-}/Zn$ [50]	−1.21 [42]	$NaOH$
Cation-based redox pair	Co^{3+}/Co^{2+} [51]	+1.95	CH_3SO_3H
	Ce_2O^{6+}/Ce^{3+}	+1.87 [43]	$HClO_4$
	Ce^{4+}/Ce^{3+} [52, 53]	+1.74	CH_3SO_3H, H_2SO_4
	Mn^{3+}/Mn^{2+} [54]	+1.54	H_2SO_4
	NpO_2^{2+}/NpO_2^+ [55]	+1.14	HNO_3
	VO_2^+/VO^{2+} [44, 56, 57]	+0.99	H_2SO_4, CH_3SO_3H
	Fe^{3+}/Fe^{2+} [1, 57-59]	+0.77	HCl
	Cu^{2+}/Cu [57]	+0.34	H_2SO_4
	Np^{4+}/Np^{3+} [55]	+0.15	HNO_3
	Sn^{4+}/Sn^{2+} [57]	+0.15	H_2SO_4
	Ti^{4+}/Ti^{3+} [1, 48]	−0.06	HCl
	V^{3+}/V^{2+} [25, 44, 59]	−0.26	H_2SO_4, HCl
	Cr^{3+}/Cr^{2+} [1, 48, 60]	−0.41	H_2SO_4, HCl
	Fe^{2+}/Fe [58]	−0.45	HCl
	Zn^{2+}/Zn [46, 47, 51, 52, 56]	−0.76	$NaBr$, $ZnCl_2$, CH_3SO_3H
Anion-cation hybrid redox pair	$Cr_2O_7^{2-}/Cr^{3+}$ [60]	+1.23	HCl
	$Cr(edta)^+/Cr(edta)^-$ [23]	+1.14†	$NaAc$

Non-ion redox pairs [61] and gas-involved redox pairs [62-66] are not included, as their RFBs may not need IEMs. Standard redox potentials are calculated from standard Gibbs free energies or cited directly from standard redox potential table [67] unless otherwise noted. Note that, when H^+ or OH^- are involved, unity of their activity was used unless otherwise noted.

* Calculated from Gibbs free energies in the reference [68].

† Calculated from formation constant of complex in the reference [69].

‡ The complex structure was taken at pH = 6 from the reference [70].

Table 2 Two application examples of double-IEM design

Application	Negative electrolyte			Middle electrolyte	Positive electrolyte			Cell parameter				
	Redox pair	Electrolyte	φ^{0*} (V)		Redox pair	Electrolyte	φ^{0*} (V)	E^0† (V)	OCV‡ (V)	CE§ (%)	VE¶ (%)	EE‖ (%)
Zn-Ce RFB	$Zn(OH)_4^{2-}/Zn$	$NaOH$	−1.21	$NaClO_4$	Ce_2O^{6+}/Ce^{3+}	$HClO_4$	+1.87	3.08	3.10	98	91	89
S-Fe RFB	S_4^{2-}/S_2^{2-}	$NaOH$	−0.45	$NaCl$	Fe^{3+}/Fe^{2+}	HCl	+0.77	1.22	1.40	100	70	70

* φ^0, standard redox potential.

† E^0, standard cell voltage.

‡ **OCV**, open circuit voltage, at 90% of SOC.

§ **CE**, round-trip columbic efficiency, 5 mA/cm^2 of charge/discharge current density.

¶ **VE**, round-trip voltage efficiency, 5 mA/cm^2 of charge/discharge current density.

‖ **EE**, round-trip energy efficiency, 5 mA/cm^2 of charge/discharge current density.

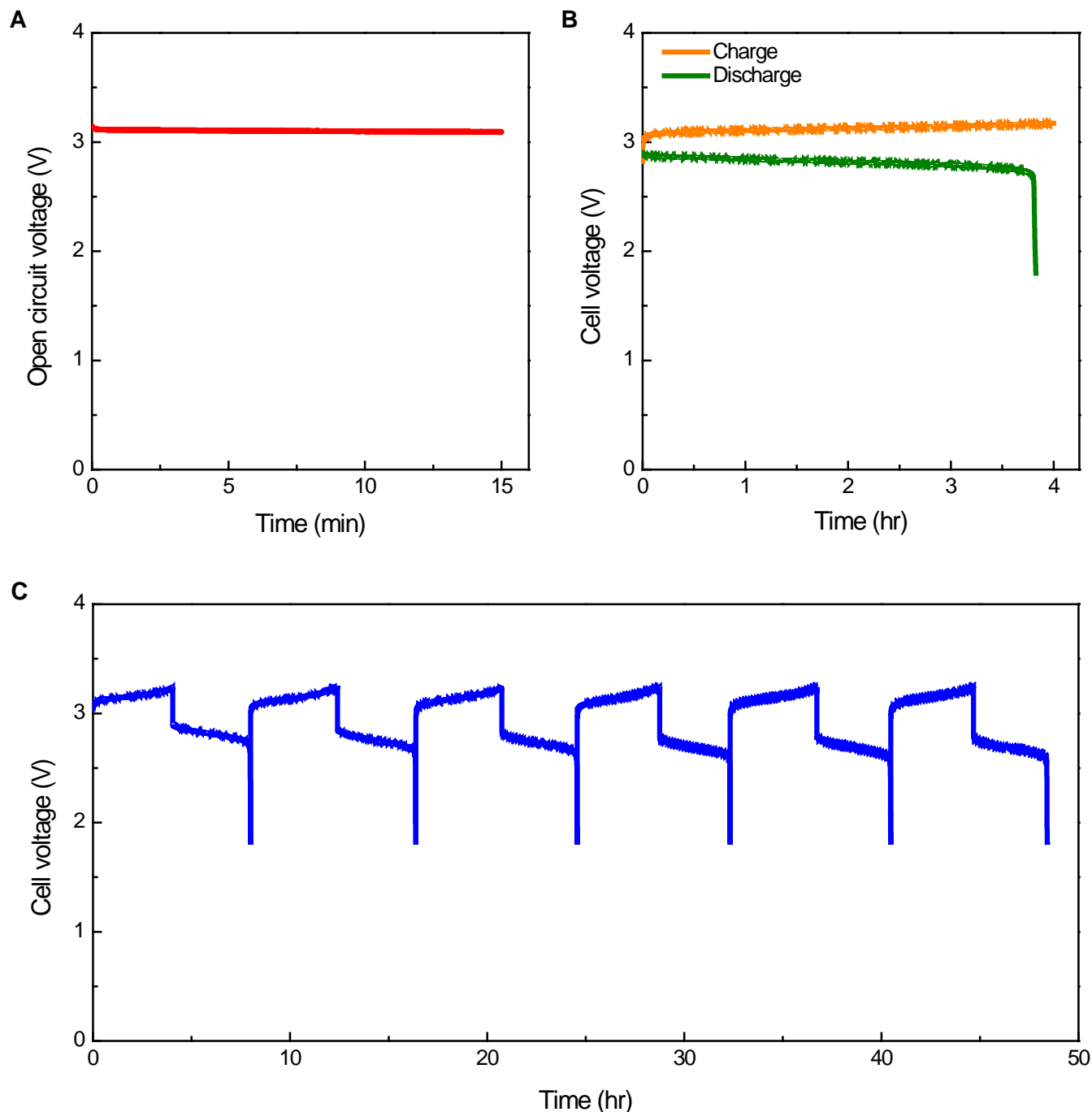Energy & Environmental Science Accepted Manuscript

Fig. 4. High-voltage RFB application of double-IEM design: the combination of zinc anion redox pair and cerium cation redox pair (Zn-Ce RFB). Cell compositions: $Zn(OH)_4^{2-}/Zn$ as negative redox pair (3 M NaOH as supporting electrolyte), Ce_2O^{6+}/Ce^{3+} as positive redox pair (2.5 M HClO$_4$ as supporting electrolyte), and 4 M NaClO$_4$ as middle electrolyte. Charge process: negative electrode, $Zn(OH)_4^{2-} + 2e^- = Zn + 4OH^-$; positive electrode, $2Ce^{3+} + H_2O = Ce_2O^{6+} + 2H^+ + 2e^-$; middle electrolyte, NaClO$_4$ concentration decreases. Discharge process is the reverse of charge process. (**A**) OCV of the basic zinc-acidic cerium double-IEM cell (90% of SOC). (**B**) Charge and discharge operation curves (5 mA/cm^2 of current density and 0−75% SOC swing). (**C**) 50-hr deep cycling performance (six complete cycles with 0−75% SOC swing). Note that the choice of NaClO$_4$ as middle electrolyte is based on its high solubility (9.93 M [67], compared with 5.65 M for CH$_3$SO$_3$Na [71]) and the high redox potential for Ce(IV)/Ce(III) in HClO$_4$ [43].

8 | *Energy & Environ. Sci.*, 2013, **00**, 1-13

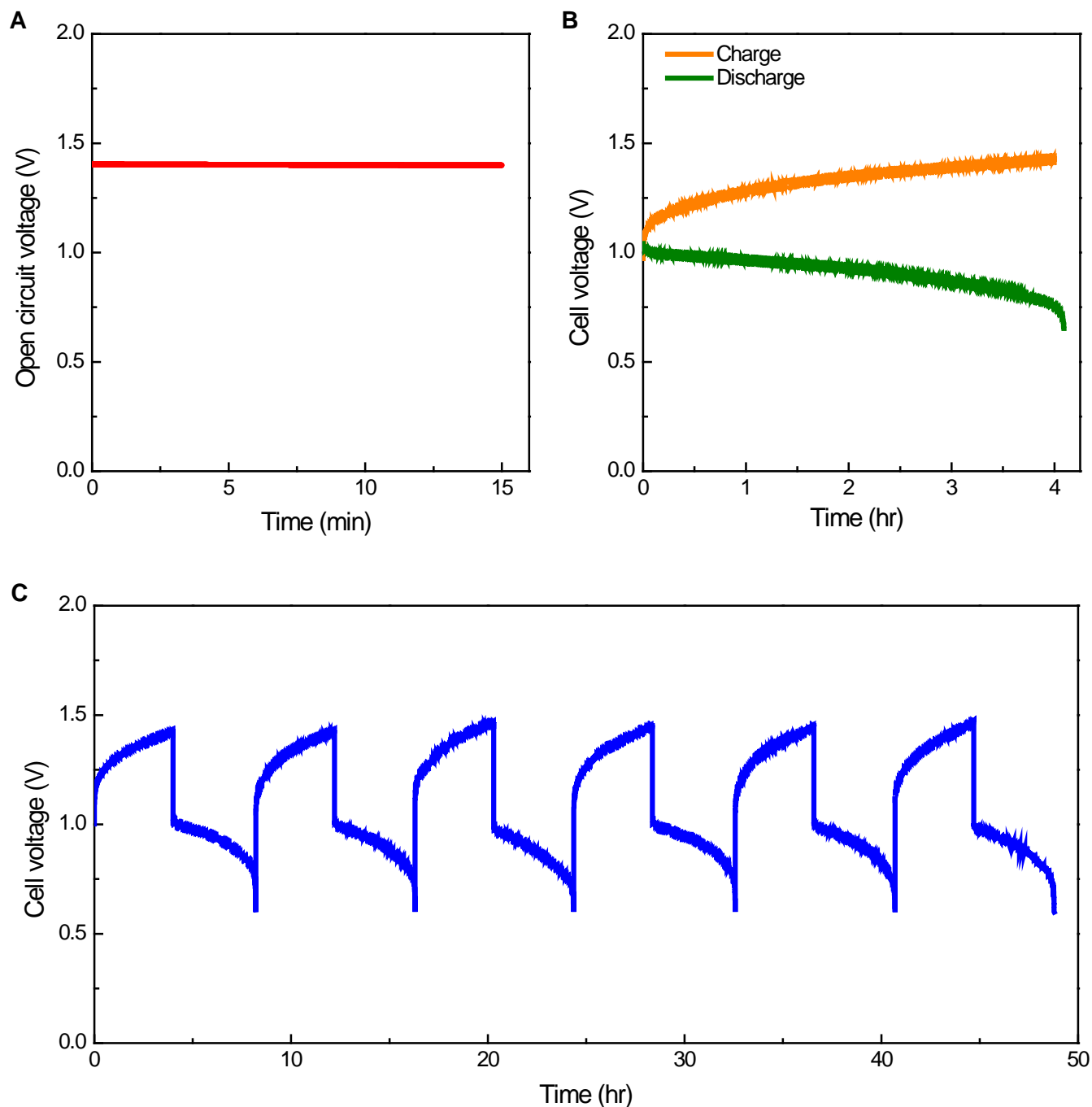This journal is © The Royal Society of Chemistry 2012

Fig. 5. Low-cost RFB application of double-IEM design: the combination of sulfur anion redox pair and iron cation redox pair (S-Fe RFB). Cell compositions: S_4^{2-}/S_2^{2-} as negative redox pair (1 M NaOH as supporting electrolyte), Fe^{3+}/Fe^{2+} as positive redox pair (1 M HCl as supporting electrolyte), and 3 M NaCl as middle electrolyte. Charge process: negative electrode, $S_4^{2-} + 2e^- = 2S_2^{2-}$; positive electrode, $Fe^{2+} = Fe^{3+} + e^-$; middle electrolyte, NaCl concentration decreases. Discharge process is the reverse of charge process. (**A**) OCV of the basic sulfur-acidic iron double-IEM cell (90% of SOC). (**B**) Charge and discharge operation curves (5 mA/cm² of current density and 0−75% SOC swing). (**C**) 50-hr deep cycling performance (six complete cycles with 0−75% SOC swing).

This journal is © The Royal Society of Chemistry 2012

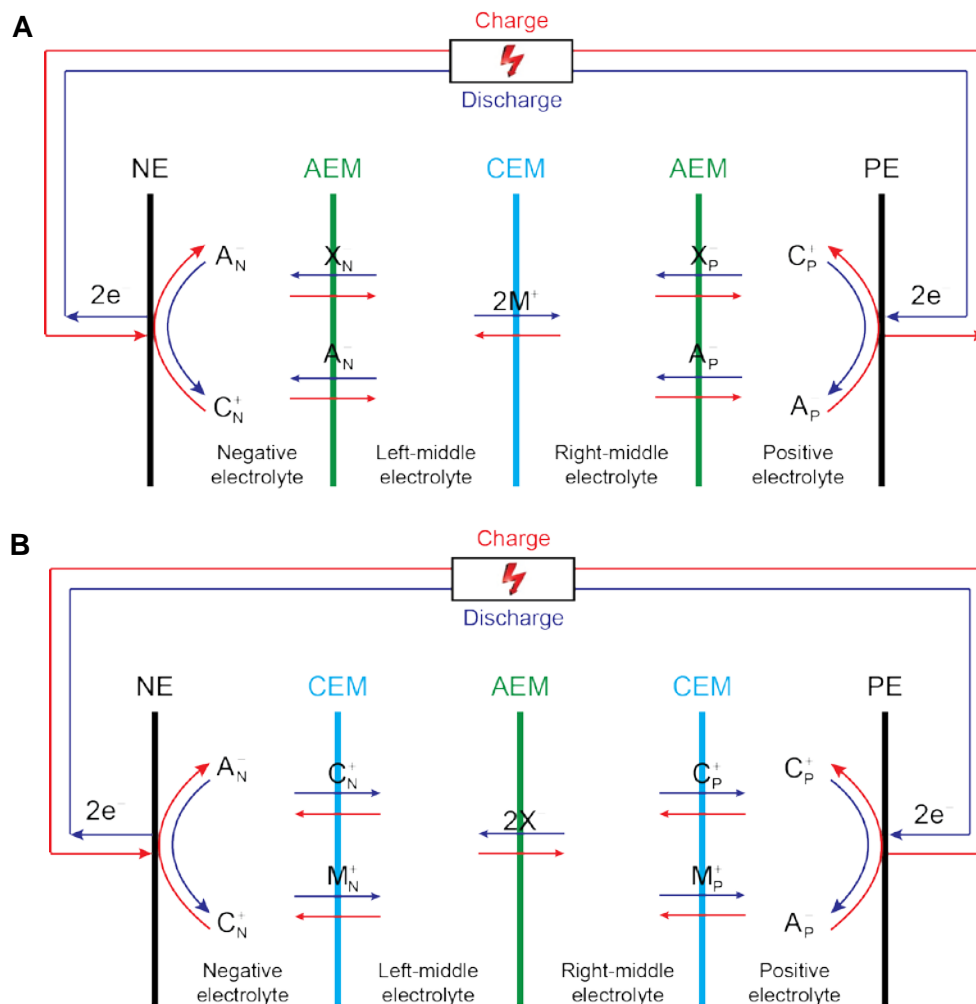*Energy & Environ. Sci.*, 2013, **00**, 1-13 | **9**

Fig. 6. Working principles of triple-IEM RFB cell configuration. NE and PE represent the negative electrode and positive electrode, respectively. (**A**) AEM-CEM-AEM configuration for the combination of an anion-cation hybrid (negative) redox pair (C_N^+/A_N^-) and another anion-cation hybrid (positive) redox pair (C_P^+/A_P^-). (**B**) CEM-AEM-CEM configuration for the same combination of the two hybrid redox pairs. M^+, M_N^+, M_P^+, X^-, X_N^-, and X_P^- are balancing ions. Note that the general working principles are, for the sake of simplicity, based on the assumptions that cations with more positive charge have higher oxidation number than those with less positive charge, and anions with more negative charge have lower oxidation number than those with less negative charge. When ions that do not follow those assumptions are used, the working principles are still applicable with minor alterations.
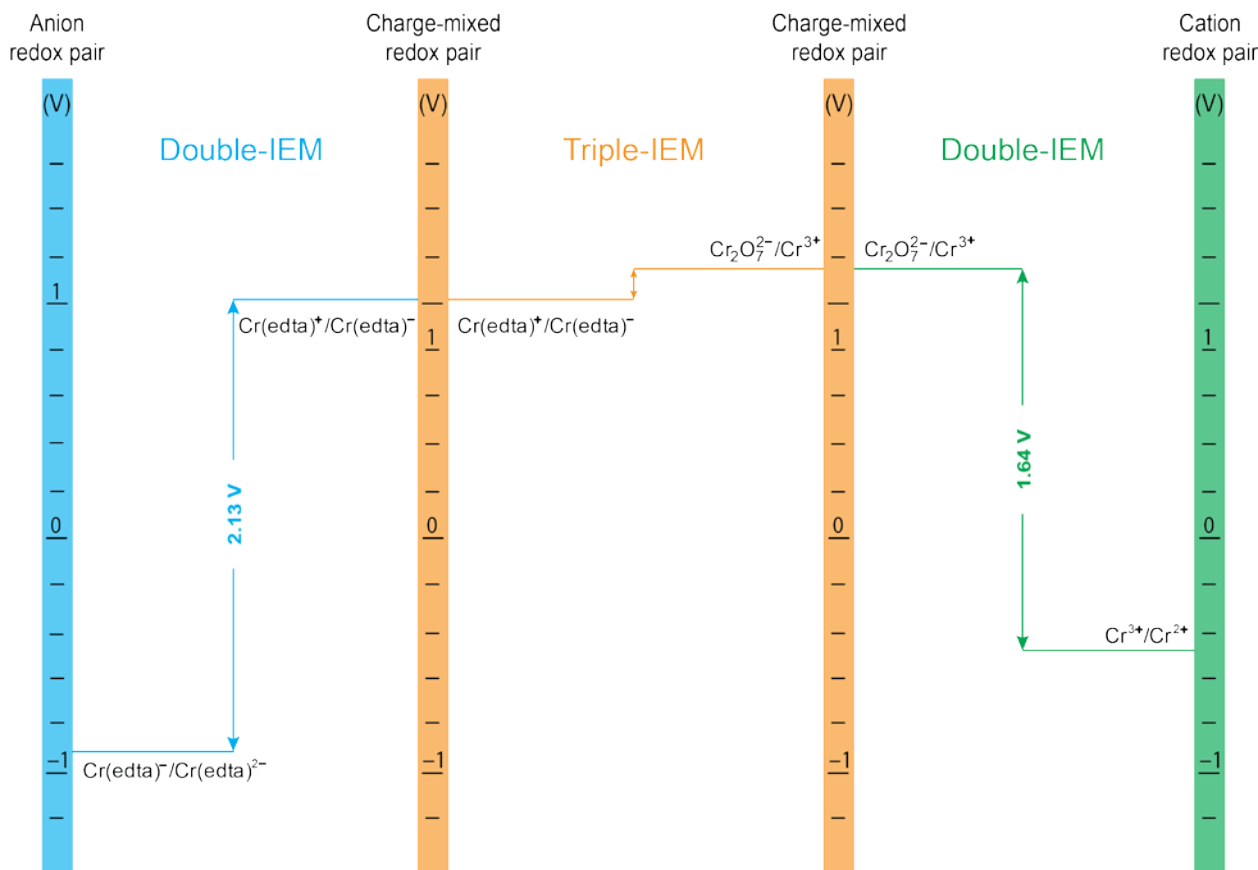
10 | *Energy & Environ. Sci.*, 2013, **00**, 1-13

This journal is © The Royal Society of Chemistry 2012

Fig. 7. Preferred cell configurations for aqueous RFBs with anion-cation hybrid redox pairs. The standard redox potentials of redox pairs are from the references in **Table 1**. Double-CEM cell is preferred for one anion/anion redox pair vs. one anion-cation hybrid redox pair (left region), and one cation/cation redox pair vs. one anion-cation hybrid redox pair (right region); and triple-AEM cell is preferred for one anion-cation hybrid redox pair vs. another anion-cation hybrid redox pair (middle region).

Discussion

The double-IEM design is general for RFBs based on an anion/anion or a cation/cation pair vs. an anion-cation hybrid pair. It is noted, however, a single-IEM cell may be sufficient here under some special conditions. A hypothetical case is shown in the **Fig. S1**. The triple-IEM is a general design for RFBs based on an anion-cation hybrid pair vs. an anion-cation hybrid pair, and similarly, a double-IEM and even a single-IEM may also be enough under some special circumstances. **Fig. S2** and **S3** show the possibilities for the two cases (double-IEM and single-IEM). Besides, the RFB configurations can also be simplified if non-ion species[61] or gas species[62-65] are involved in redox pairs.

Enabled by the effective redox pair isolation and ion buffer function provided by the additional middle electrolyte, the double-IEM or triple-IEM cells also offer significantly lower overall ion crossover rate between negative and positive electrolyte than single-IEM cells (15−143 times slower for double-IEM and 150−4177 times slower for triple-IEM, at given 1−100 ppm threshold of overall ion crossover, **Text S1**, **Fig. S4A** and **Table S1**). At the same time, the energy capacity will remain the same for both double-IEM & triple-IEM configuration and single-IEM one, if IEMs used have the same quality in each configuration.

Owing to the ultra-low overall ion crossover rate, the thickness of IEMs used in double-IEM and triple-IEM RFBs can be reduced without significantly compromising the coulombic efficiency. The use of thin IEMs enables the reduction of the overall cell internal resistance (e.g., to the same level of single-IEM cases), promising to deliver high current density without large loss in efficiency or durability. For instance, with one half or one third of the thickness, the overall membrane resistance in double-IEM or triple-IEM cell remains roughly the same as that of single-IEM cases, but the overall ion crossover rate is still 7.5−71 times slower for double-IEM or 82−1392 times slower for triple-IEM simulated, at given 1−100 ppm threshold of overall ion crossover (**Text S1**, **Fig. S4B** and **Table S2**).

Besides providing the function of electrolyte continuity and serving as ion crossover buffer, the middle electrolyte provides another significant benefit for RFBs based on an anion/anion redox pair vs. a cation/cation pair: cleaning of crossovered ions-contaminated electrolytes in negative and positive electrolytes. Low level crossovered ions (e.g., 100 ppm) can be easily removed from the contaminated electrolytes by refreshing the middle electrolytes, because the crossovered ions will rapidly diffuse back to the fresh middle electrolytes under the established ion concentration difference. Such a cleaning function helps drastically extend the cell lifetime. In addition, the middle electrolyte also offers a possibility to manage the possible water solvent transfer issues among

electrolytes, by tuning its salt concentration (a wide range of salt concentration in middle electrolyte is allowed depending the SOC swing) and its volume ratio (to negative electrolyte or positive electrolyte).

A low current density (5 mA/cm^2) used here is sufficient for the concept validation in this work but low for practical applications. Higher current densities (e.g., 20−50 mA/cm^2) can be carried out but the voltage efficiency is compromised due to the large internal resistance (around 18−20 Ωcm^2 measured). The large internal resistance also explains why the sulfur-iron RFB has lower voltage efficiency than the zinc-cerium because the similar internal resistance-caused voltage loss accounts for a larger portion in a lower voltage of the sulfur-iron RFB (**Table 2**). The non-optimized cell structures are mainly responsible for the large internal resistance observed. For example, the large thickness of electrolytes (**1 cm each**) leads to a calculated total resistance of 12−14 Ωcm^2. Membrane resistance and mass-transport resistance especially in the middle electrolyte can also contribute. It is clear that an optimized cell structure can drastically reduce the cell resistance, allowing high current density operations without a significant voltage efficiency penalty. It is also noted here that the extra membrane and electrolyte in a double-IEM adds complexity to the RFB system in terms of cell assembly, electrolyte management, and system operation. These complexities however can be managed through innovative cell designs.

The double-IEM configuration should not be limited to aqueous RFBs, and may be applicable for non-aqueous RFBs based on mixed ion charges, such as non-aqueous all-ruthenium RFB (Ru(acac)$_3$/[Ru(acac)$_3$]$^-$ vs. [Ru(acac)$_3$]$^+$/Ru(acac)$_3$) [72], all-vanadium RFB (V(acac)$_3$/[V(acac)$_3$]$^-$ vs. [V(acac)$_3$]$^+$/V(acac)$_3$) [73], all-chromium RFB ([Cr(acac)$_3$]$^-$/[Cr(acac)$_3$]$^{2-}$ vs. [Cr(acac)$_3$]$^+$/Cr(acac)$_3$) [74], and all-magnesium RFB (Mn(acac)$_3$/[Mn(acac)$_3$]$^-$ vs. [Mn(acac)$_3$]$^+$/Mn(acac)$_3$) [75].

Conclusions

In summary, multiple IEMs (double-IEM and triple-IEM) cell configurations are introduced to RFBs. The multiple-IEM cell configurations bring unprecedented freedom to construct RFBs with any combinations of mixed ion charges and electrolytes. Two featured RFBs based on the multiple-IEM cell design are also demonstrated: (i) ultra-high voltage zinc-cerium RFB and (ii) ultra-low cost sulfur-iron RFBs. With multiple IEMs cell configuration, many other featured RFBs constructed by redox pairs with mixed ion charges are also possible.

Acknowledgements

References

1. L. H. Thaller, *The 9th Intersociety Energy Conversion Engineering Conference Proceedings*, 1974, 924-928.
2. Y. Z. Liu, Y. F. Li, M. Zhong, Y. G. Yang, Y. F. Wen and M. Z. Wang, *J Mater Chem*, 2011, **21**, 15449-15455.
3. B. Dunn, H. Kamath and J. M. Tarascon, *Science*, 2011, **334**, 928-935.
4. W. A. Braff, M. Z. Bazant and C. R. Buie, *Nat Commun*, 2013, **4**.
5. B. Huskinson, M. P. Marshak, C. Suh, S. Er, M. R. Gerhardt, C. J. Galvin, X. Chen, A. Aspuru-Guzik, R. G. Gordon and M. J. Aziz, *Nature*, 2014, **505**, 195-198.
6. C. P. de Leon, A. Frias-Ferrer, J. Gonzalez-Garcia, D. A. Szanto and F. C. Walsh, *J Power Sources*, 2006, **160**, 716-732.
7. M. Skyllas-Kazacos, M. H. Chakrabarti, S. A. Hajimolana, F. S. Mjalli and M. Saleem, *J Electrochem Soc*, 2011, **158**, R55-R79.
8. A. Z. Weber, M. M. Mench, J. P. Meyers, P. N. Ross, J. T. Gostick and Q. H. Liu, *J Appl Electrochem*, 2011, **41**, 1137-1164.
9. X. F. Li, H. M. Zhang, Z. S. Mai, H. Z. Zhang and I. Vankelecom, *Energy Environ Sci*, 2011, **4**, 1147-1160.
10. B. Schwenzer, J. L. Zhang, S. Kim, L. Y. Li, J. Liu and Z. G. Yang, *Chemsuschem*, 2011, **4**, 1388-1406.
11. P. Leung, X. H. Li, C. P. de Leon, L. Berlouis, C. T. J. Low and F. C. Walsh, *RSC Adv*, 2012, **2**, 10125-10156.
12. W. Wang, Q. T. Luo, B. Li, X. L. Wei, L. Y. Li and Z. G. Yang, *Adv Funct Mater*, 2013, **23**, 970-986.
13. R. Ferrigno, A. D. Stroock, T. D. Clark, M. Mayer and G. M. Whitesides, *J Am Chem Soc*, 2002, **124**, 12930-12931.
14. Y. H. Lu, J. B. Goodenough and Y. Kim, *J. Am. Chem. Soc.*, 2011, **133**, 5756-5759.
15. Y. R. Wang, Y. G. Wang and H. S. Zhou, *ChemSusChem*, 2011, **4**, 1087-1090.
16. F. R. Brushett, J. T. Vaughey and A. N. Jansen, *Adv. Energy Mater.*, 2012, **2**, 1390-1396.
17. K. J. Kim, M. S. Park, J. H. Kim, U. Hwang, N. J. Lee, G. Jeong and Y. J. Kim, *Chem Commun*, 2012, **48**, 5455-5457.
18. W. Wang, W. Xu, L. Cosimbescu, D. W. Choi, L. Y. Li and Z. G. Yang, *Chem Commun*, 2012, **48**, 6669-6671.
19. Q. T. Luo, L. Y. Li, W. Wang, Z. M. Nie, X. L. Wei, B. Li, B. W. Chen, Z. G. Yang and V. Sprenkle, *Chemsuschem*, 2013, **6**, 268-274.
20. B. Li, M. Gu, Z. Nie, Y. Shao, Q. Luo, X. Wei, X. Li, J. Xiao, C. Wang, V. Sprenkle and W. Wang, *Nano Lett*, 2013, **13**, 1330-1335.
21. J. Liu, J. G. Zhang, Z. G. Yang, J. P. Lemmon, C. Imhoff, G. L. Graff, L. Y. Li, J. Z. Hu, C. M. Wang, J. Xiao, G. Xia, V. V. Viswanathan, S. Baskaran, V. Sprenkle, X. L. Li, Y. Y. Shao and B. Schwenzer, *Adv Funct Mater*, 2013, **23**, 929-946.
22. S. H. Shin, S. H. Yun and S. H. Moon, *RSC Adv*, 2013, **3**, 9095-9116.
23. C. H. Bae, E. P. L. Roberts and R. A. W. Dryfe, *Electrochim Acta*, 2002, **48**, 279-287.
24. C. H. Bae, E. P. L. Roberts, M. H. Chakrabarti and M. Saleem, *Int J Green Energy*, 2011, **8**, 248-264.
25. M. Skyllas-Kazacos, *J. Power Sources*, 2003, **124**, 299-302.
26. H. Vafiadis and M. Skyllas-Kazacos, *J. Membr. Sci.*, 2006, **279**, 394-402.
27. G. M. Weng, C. Y. V. Li and K. Y. Chan, *ECS Trans.*, 2013, **53**, 39-50.
28. G. M. Weng, C. Y. V. Li and K. Y. Chan, *J. Electrochem. Soc.*, 2013, **160**, A1384-A1389.
29. H. Strathmann, J. J. Krol, H. J. Rapp and G. Eigenberger, *J. Membr. Sci.*, 1997, **125**, 123-142.
30. J. J. Krol, M. Jansink, M. Wessling and H. Strathmann, *Sep. Purif. Technol.*, 1998, **14**, 41-52.
31. T. Aritomi, T. vandenBoomgaard and H. Strathmann, *Desalination*, 1996, **104**, 13-18.

32. H. Q. Li, G. M. Weng, C. Y. V. Li and K. Y. Chan, *Electrochim. Acta*, 2011, **56**, 9420-9425.

33. *USA Pat.*, 7,344,801, 2008.

34. K. Y. Chan and S. A. Cheng, *ECS Trans.*, 2010, **25**, 213-219.

35. Y. Ayato, T. Okada and Y. Yamazaki, *Electrochemistry*, 2003, **71**, 313-317.

36. M. Unlu, J. F. Zhou and P. A. Kohl, *Angewandte Chemie-International Edition*, 2010, **49**, 1299-1301.

37. P. Murray, *Electrodialysis and Electrodialysis Reversal*, American Water Works Assn, 1995.

38. G. M. Weng, C. Y. V. Li and K. Y. Chan, *ECS Trans.*, 2012, **41**, 133-143.

39. J. Cheng, L. Zhang, Y. S. Yang, Y. H. Wen, G. P. Cao and X. D. Wang, *Electrochem. Commun.*, 2007, **9**, 2639-2642.

40. P. K. Leung, C. Ponce-de-Leon, C. T. J. Low, A. A. Shah and F. C. Walsh, *J. Power Sources*, 2011, **196**, 5174-5185.

41. P. Zhao, H. M. Zhang, H. T. Zhou and B. L. Yi, *Electrochim. Acta*, 2005, **51**, 1091-1098.

42. T. P. Dirkse, *J Electrochem Soc*, 1954, **101**, 328-331.

43. E. Wadsworth, F. R. Duke and C. A. Goetz, *Anal Chem*, 1957, **29**, 1824-1825.

44. M. Skyllas-Kazacos, M. Rychcik, R. G. Robins, A. G. Fane and M. A. Green, *J Electrochem Soc*, 1986, **133**, 1057-1058.

45. *USA Pat.*, 4485154, 1984.

46. L. Q. Zhang, Q. Z. Lai, J. L. Zhang and H. M. Zhang, *Chemsuschem*, 2012, **5**, 867-869.

47. H. S. Lim, A. M. Lackner and R. C. Knechtli, *J Electrochem Soc*, 1977, **124**, 1154-1157.

48. *Japan Pat.*, 57009072, 1982.

49. Y. H. Wen, H. M. Zhang, P. Qian, H. T. Zhou, P. Zhao, B. L. Yi and Y. S. Yang, *J Electrochem Soc*, 2006, **153**, A929-A934.

50. G. B. Adams, R. P. Hollandsworth and E. L. Littauer, *Proceedings of the 16th Intersociety Energy Conversion Engineering Conference*, 1981, 812-816.

51. *USA Pat.*, 6986966, 2006.

52. *USA Pat.*, 7625663, 2004.

53. B. Fang, S. Iwasa, Y. Wei, T. Arai and M. Kumagai, *Electrochim Acta*, 2002, **47**, 3971-3976.

54. F. Q. Xue, Y. L. Wang, W. H. Wang and X. D. Wang, *Electrochim Acta*, 2008, **53**, 6636-6642.

55. T. Yamamura, N. Watanabe, T. Yano and Y. Shiokawa, *J Electrochem Soc*, 2005, **152**, A830-A836.

56. C. Tang and D. B. Zhou, *Electrochim Acta*, 2012, **65**, 179-184.

57. D. G. Oei, *J Appl Electrochem*, 1982, **12**, 41-51.

58. L. W. Hruska and R. F. Savinell, *J Electrochem Soc*, 1981, **128**, 18-25.

59. W. Wang, S. Kim, B. Chen, Z. Nie, J. Zhang, G.-G. Xia, L. Li and Z. Yang, *Energy Environ Sci*, 2011, **4**, 4068-4073.

60. J. Doria, M. C. D. Andres and C. Armenta, *NTERSOL 85: Proceedings of the Ninth Biennial Congress of the International Solar Energy Society*, 1985, 1500.

61. Y. Xu, Y. H. Wen, J. Cheng, G. P. Cao and Y. S. Yang, *Electrochem Commun*, 2009, **11**, 1422-1424.

62. R. F. Savinell and D. A. Polaski, *Proceedings of the 16th Intersociety Energy Conversion Engineering Conference*, 1981, **1**, 817.

63. E. Gileadi, S. Srinivasan, F. J. Salzano, C. Braun, A. Beaufrere, S. Gottesfeld, L. J. Nuttall and A. B. Laconti, *J Power Sources*, 1977, **2**, 191-200.

64. *Japan Pat.*, 60227364, 1985.

65. R. S. Yeo and D. T. Chin, *J Electrochem Soc*, 1980, **127**, 549-555.

66. C. Menictas and M. Skyllas-Kazacos, *J. Appl. Electrochem.*, 2011, **41**, 1223-1232.

67. D. R. Lide, *CRC Handbook of Chemistry and Physics*, CRC Press, Bora Raton, FL, 2007.

68. V. E. Mironov and N. P. Lastovkina, *Russ J Phys Chem+*, 1967, **41**, 991.

69. J. A. Dean, *Lange's Handbook of Chemistry*, McGraw, 1998.

70. J. L. Pierre and I. Gautier-Luneau, *Biometals*, 2000, **13**, 91-96.

71. M. D. Gernon, M. Wu, T. Buszta and P. Janney, *Green Chem.*, 1999, **1**, 127-140.

72. M. H. Chakrabarti, R. A. W. Dryfe and E. P. L. Roberts, *Electrochim Acta*, 2007, **52**, 2189-2195.

73. Q. H. Liu, A. E. S. Sleightholme, A. A. Shinkle, Y. D. Li and L. T. Thompson, *Electrochem Commun*, 2009, **11**, 2312-2315.

74. Q. H. Liu, A. A. Shinkle, Y. D. Li, C. W. Monroe, L. T. Thompson and A. E. S. Sleightholme, *Electrochem Commun*, 2010, **12**, 1634-1637.

75. A. E. S. Sleightholme, A. A. Shinkle, Q. H. Liu, Y. D. Li, C. W. Monroe and L. T. Thompson, *J Power Sources*, 2011, **196**, 5742-5745.

This journal is © The Royal Society of Chemistry 2012

Energy & Environ. Sci., 2013, **00**, 1-13 | **13**

Electronic Supplementary Information for

# A multiple ion-exchange membrane design for redox flow batteries

Shuang Gu*, Ke Gong, Emily Z. Yan & Yushan Yan*

Department of Chemical & Biomolecular Engineering, Center for Catalytic Science and Technology, University of Delaware, Newark, DE 19716, USA.

Correspondence and requests for materials should be addressed to S.G. (email: shgu@udel.edu) or to Y.S.Y. (email: yanys@udel.edu)

Text S1. Comparison of ion crossover of double-IEM and triple-IEM over single-IEM cell configuration

Assumptions are as follows: (1) The concentration of all ions in their electrolytes is uniform; (2) The volume of all electrolytes is the same; (3) The diffusion coefficient of all anions in the AEM is the same and also equals to the diffusion coefficient of all cations in the CEM; and (4) The ion selectivity of AEM for the anion and CEM for the cation is 99% (i.e., the diffusion coefficient of any anion is 99 times that of any cation in AEM, and the diffusion coefficient of any cation is 99 times that any anion in CEM).
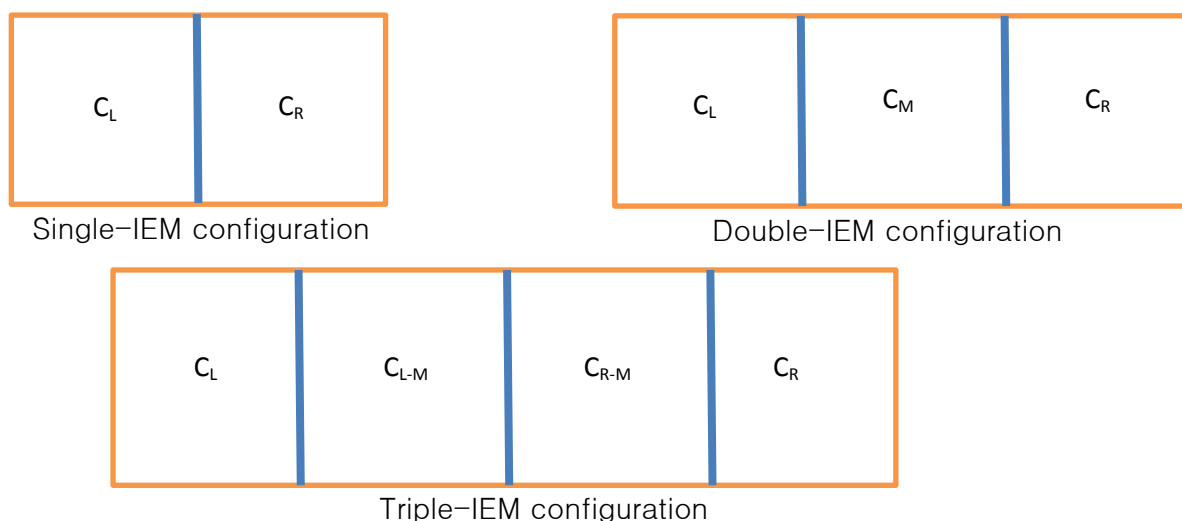
Scheme S1. Configuration of single-IEM, double-IEM, and triple-IEM RFBs.

With the aforementioned assumptions, the crossover behavior of electro-active ions in each side of the RFB becomes symmetric. We consider the following crossover as an example for analysis: Electro-active anion crossovers from left side to the right side of a RFB cell. The following differential equations can be established for each case (**Scheme S1**).

(i) Single-IEM configuration:

$$\frac{dC_L}{dt} = -\frac{D_{-+}}{d_1}(C_L - C_R)$$

$$\frac{dC_R}{dt} = \frac{D_{-+}}{d_1}(C_L - C_R)$$

(ii) Double–IEM configuration:

$$\frac{dC_L}{dt} = -\frac{D_{-+}}{d_2}(C_L - C_M)$$

$$\frac{dC_M}{dt} = \frac{D_{-+}}{d_2}(C_L - C_M) - \frac{D_{--}}{d_2}(C_M - C_R)$$

$$\frac{dC_R}{dt} = \frac{D_{--}}{d_2}(C_M - C_R)$$

(iii)Triple–IEM configuration:

$$\frac{dC_L}{dt} = -\frac{D_{-+}}{d_3}(C_L - C_{L-M})$$

$$\frac{dC_{L-M}}{dt} = \frac{D_{-+}}{d_3}(C_L - C_{L-M}) - \frac{D_{--}}{d_3}(C_{L-M} - C_{R-M})$$

$$\frac{dC_{R-M}}{dt} = \frac{D_{--}}{d_3}(C_{L-M} - C_{R-M}) - \frac{D_{-+}}{d_3}(C_{R-M} - C_R)$$

$$\frac{dC_R}{dt} = \frac{D_{-+}}{d_3}(C_{R-M} - C_R)$$

Where, D_+ and D_- are diffusion coefficients of the electro–active anion in CEM and AEM, respectively; C_L, C_R, C_M, C_{L-M}, C_{R-M} are the concentrations of the anion in left electrolyte, right electrolyte, middle electrolyte, left–middle electrolyte, and right–middle electrolyte, respectively; d_1, d_2, and d_3 are IEM thickness in single–IEM, double–IEM, and triple–IEM, respectively; and t is time.

The concentration of the electro–active anion in left electrolyte is one unit and zero in all other electrolytes at time zero. For the double–IEM configuration, two IEM thicknesses are considered: 1) the same and 2) a half of the single–IEM thickness. For triple–IEM configuration two IEM thicknesses are also considered: 1) the same and 2) a third of the single–IEM thickness. With these assumptions above conditions, the differential equations listed above were solved by Matlab®, and the results are shown in **Figure S4** and **Table S1** and **S2**.

Table S1. Crossover time ratios of double-IEM and triple-IEM over single-IEM cell configuration to reach a given crossover tolerance ($d_1 = d_2 = d_3$)			
Cell configuration	Crossover time ratio under given crossover tolerance		
	1 ppm	10 ppm	100 ppm
Double-IEM over single-IEM	142	46	15
Triple-IEM over single-IEM	4177	976	150

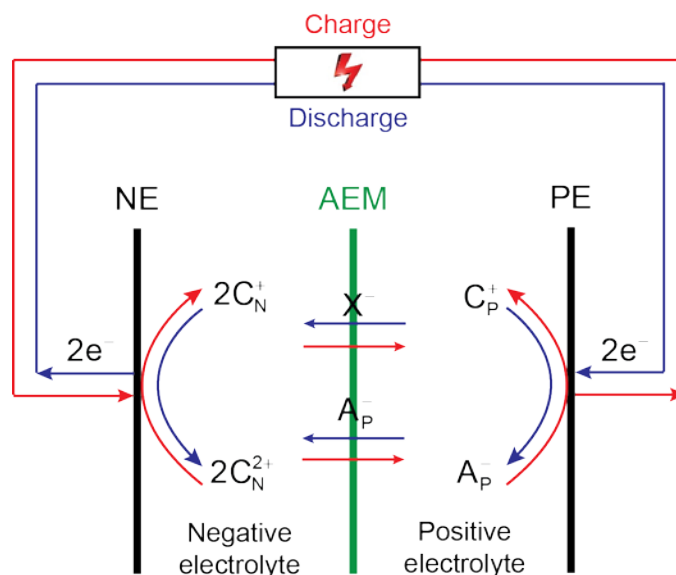| Table S2. Crossover time ratios of double-IEM and triple-IEM over single-IEM cell configuration to reach a given crossover tolerance [$d_2 = (1/2) d_1$ and $d_3 = (1/3) d_1$]			
Cell configuration	Crossover time ratio under given crossover tolerance		
	1 ppm	10 ppm	100 ppm
Double-IEM over single-IEM	71	23	7.5
Triple-IEM over single-IEM	1393	326	82

Fig. S1. Schematic of a possible single–IEM RFB that is capable of handling a cation/cation redox pair (or anion/anion pair) vs. an anion–cation hybrid redox pair. A cation/cation redox pair (C_N^{2+}/C_N^+) in negative electrolyte vs. a cation/anion hybrid redox pair (C_P^+/A_P^-) in positive electrolyte. X^- is the balancing anion. When A_P^- does not react with either C_N^+ or C_N^{2+} (no electrochemical reaction or other chemical reactions), a single AEM can be sufficient for this RFB, although a double–IEM configuration is preferred. For an anion/anion negative pair vs. an anion/cation hybrid positive pair, a CEM can be sufficient.
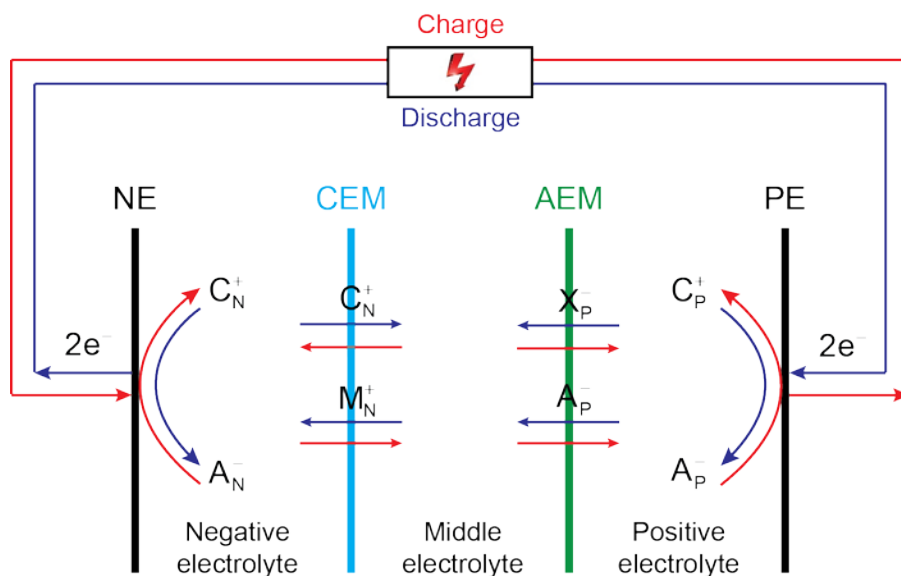
Fig. S2. Schematic of a possible double−IEM RFB that is capable of handling an anion−cation hybrid redox pair vs. an anion−cation hybrid redox pair. An anion/cation hybrid redox pair (A_N^-/C_N^+) in negative electrolyte vs. a cation/anion hybrid redox pair (C_P^+/A_P^-) in positive electrolyte. M_N^+ and X_P^- are the balancing ions. When C_N^+ and A_P^- do not react with each other, a double−IEM (CEM/AEM combination) is sufficient for this RFB, although a triple−IEM configuration is preferred.
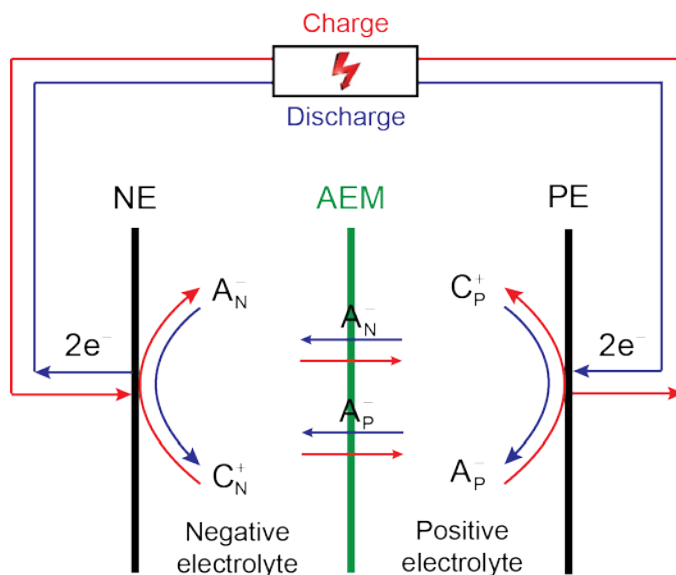
Fig. S3. Schematic of a possible single–IEM RFB that is capable of handling an anion–cation hybrid redox pair vs. an anion–cation hybrid redox pair. A carion/anion hybrid redox pair (C_N^+/A_N^-) in negative electrolyte vs. a cation/anion hybrid redox pair (C_P^+/A_P^-) in positive electrolyte. When (1) A_N^- does not react with C_P^+; (2) A_P^- does not react with C_N^+; and (3) A_N^- does not react with A_P^-, a single AEM is sufficient for this RFB, although a triple–IEM configuration is preferred.
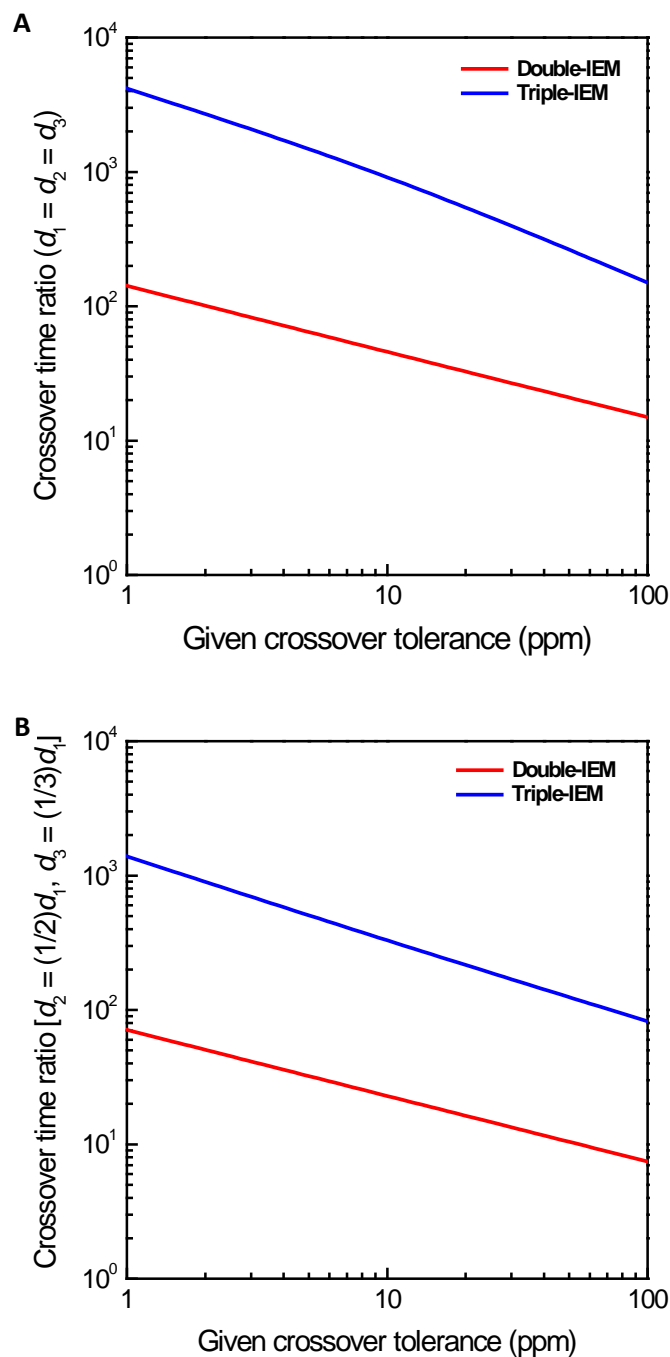
Fig. S4. The crossover time ratio of double−IEM or triple−IEM to single−IEM cell configuration. (a) The crossover time ratio of double−IEM to single−IEM cell configuration to reach a given crossover tolerance. The membranes in the double−IEM configuration have either the same thickness (red line) or a half of the single−IEM membrane thickness (blue line). (b) The crossover time ratio of triple−IEM to single−IEM cell configuration to reach a given crossover tolerance. The membranes in triple−IEM configuration have either the same thickness (red line) or a third of the single−IEM membrane thickness (blue line).
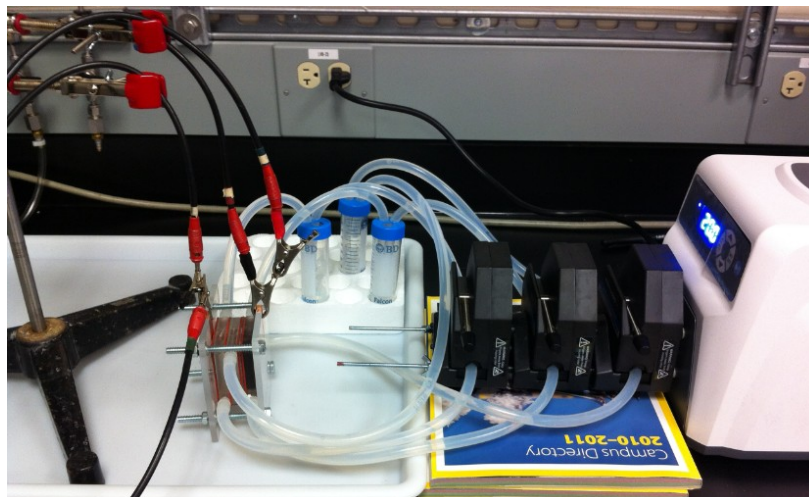
Fig. S5. Experimental setup of double−IEM cell configuration.

Broader Context (no more than 200 words):

Redox flow batteries (RFBs) are considered as the most promising technology for economical and scalable electricity storage for wind and solar energy. By decoupling the energy storage and the power delivery from each other, RFBs hold a level of design flexibility and system scalability unavailable to traditional rechargeable batteries. Since their invention, RFBs have stayed with single ion-exchange membrane (single-IEM) configuration that cannot effectively use redox pairs with mixed charges and/or supporting electrolytes with different pHs. In this work, we show a universal design concept based on a multiple-IEM configuration (double-IEM or triple-IEM) that brings unprecedented freedom in choosing both redox pairs and supporting electrolytes. Two aqueous RFB examples are featured: (1) ultra-high voltage zinc-cerium RFB with a standard cell voltage of 3.08 V, the highest among all known aqueous RFBs; and (2) ultra-low cost sulfur-iron RFB with a standard cell voltage of 1.22 V, based on two highly available electroactive elements (iron and sulfur being the 1_{st} and 5_{th} most produced elements worldwide, respectively). The multiple-IEM concept is general and can be applied to non-aqueous RFBs.